JOURNAL OF THERMOPHYSICS AND HEAT TRANSFER
Vol. 7, No. 4, Oct.–Dec. 1993

Measurement and Prediction of Dynamic Temperatures in Unsymmetrically Cooled Glass Windows

Robert E. Field*
Northern Illinois University, DeKalb, Illinois 60115
and
Raymond Viskanta†
Purdue University, West Lafayette, Indiana 47907

Semitransparent materials, such as glass, have many applications in high-temperature environments such as supersonic aircraft canopies and spacecraft windows. At elevated temperatures the energy transfer within semitransparent materials is dominated by radiation, making both the prediction and measurement of internal temperatures substantially more difficult than for opaque substances. Experimental measurement of the dynamic internal temperature distribution in soda-lime glass plates cooling from an initial temperature of ~550°C has been carried out. The boundary conditions on the plates were established using the laboratory ambient for the front surface and employing a radiant heater at the rear surface. The surface and internal plate temperatures were measured using thermocouples fused in the glass. The temperature data are compared to predictions obtained from the solution of the transient energy equation where the internal radiative transfer has been accounted for using rigorous radiative transfer theory. The predicted and measured temperatures, experimental method, process used to fuse the thermocouples in the test plates, and the formulation of the energy equation for semitransparent materials are discussed.

Nomenclature

C = specific heat
c = velocity of light
c_0 = velocity of light in free space
$E_n(t)$ = exponential function, $\int_0^1 \mu^{n-2} e^{-t/\mu}\, d\mu$
F = radiant flux
$F_{C\nu}$ = radiant flux component, Eq. (5)
$F_{H\nu}$ = radiant flux component, Eq. (9)
g = blackbody fraction, Eq. (4)
h = Planck's constant or convective heat transfer coefficient
$I_{b\nu}(T)$ = Planck's function, $2h\nu^3/c_0^2[\exp(h\nu/kT) - 1]$
I_ν = spectral intensity of radiation
k = thermal conductivity
L = thickness of layer of semitransparent medium
n = index of refraction
$R_{n,i}$ = reflection function, Eq. (10)
$R_{n,ij}$ = reflection function, Eq. (11)
T = temperature
TC = thermocouple data
$T_{n,i}$ = transmission function, Eq. (6)
$T_{n,ij}$ = transmission function, Eq. (7)
t = time
y = y coordinate direction or depth
β = function, Eq. (8)
γ = density
ε = emissivity
θ = angle between normal and pencil of radiation
κ = absorption coefficient
μ = direction cosine in semitransparent medium, $\cos\theta$
μ' = direction cosine in surrounding media, $\cos\theta'$
ν = frequency
$\rho(\mu)$ = reflectivity, $\frac{1}{2}\{[(\mu - \sqrt{\mu^2 - \mu_c^2})/(\mu + \sqrt{\mu^2 - \mu_c^2})]^2 + \{[\mu(1-\mu) - \sqrt{\mu^2 - \mu_c^2}]/[\mu(1-\mu) + \sqrt{\mu^2 - \mu_c^2}]\}^2\}$
$\tau_{L\nu}$ = optical thickness, $\int_0^L \kappa_\nu(y)\, dy$

Subscripts
a = ambient
c = critical angle, cutoff
s = surroundings
y = coordinate direction
ν = refers to frequency
0 = refers to the external media
1 = refers to the interface between a semitransparent solid and surrounding medium
2 = refers to the interface between a semitransparent solid and surrounding medium

Superscripts
0 = refers to incident flux
′ = refers to external conditions

Received July 17, 1992; revision received Nov. 30, 1992; accepted for publication Dec. 2, 1992.

*Assistant Professor, Department of Mechanical Engineering.
†W. F. M. Gross Distinguished Professor of Engineering, School of Mechanical Engineering, 1288 Mechanical Engineering Building. Fellow AIAA.

Introduction

HIGH-TEMPERATURE windows are required in applications such as supersonic aircraft canopies, spacecraft windows, and industrial process furnaces. All applications such as these result in unsymmetric heat transfer boundary conditions being imposed on the glass. Unsymmetric heating or cooling naturally produces a nonsymmetric temperature distribution in the window. The internal temperature distribution in the glass of these windows must be estimated using theoretical models. The objectives of the research reported here were to experimentally measure the dynamic temperature distribution in glass plates allowed to cool under nonsymmetric boundary conditions, and to validate the energy equation-based model through the comparison of predicted temperatures with experimental data. The validated model may then be used as a tool in a wide range of applications to predict the internal temperature distribution in plates of

semitransparent materials that are being either heated or cooled. The methods generally used in glass temperature measurement are contact thermocouples and radiation pyrometers.[1,2] For the most part, both pyrometers and thermocouples are limited to surface temperature measurement. There is scant data available in the literature where experimentally measured internal glass temperatures have been reported for dynamic conditions. The scarcity of reliable internal temperature data makes validating a theoretical model prediction of the internal glass temperature distribution very difficult. It is hoped that the data presented herein will be of use in the validation of other models.

Conduction is the diffusive transfer of energy at the molecular (phonon) level, while radiation is the transport of energy by electromagnetic waves over a finite distance. In opaque substances, conduction is the only mechanism by which heat is transferred throughout the interior; however, in semitransparent materials, energy is transferred by both conduction and radiation. The semitransparent character of glass makes internal radiative transfer a very important component of the overall heat transfer. Prediction of the dynamic temperature distribution in glass requires proper accounting of the radiant energy transfer throughout the interior of the glass, as well as conduction. Because thermal radiation is simultaneously emitted and reabsorbed within a semitransparent material, it is a bulk rather than local phenomenon. The bulk nature of the radiative energy transfer makes the analysis and experimental determination of the energy transfer in a radiatively participating material quite complex.[3,4]

Early attempts to predict[5] and measure[6,7] the temperature distribution in sheets of glass have been reported. Beattie and Coen,[6] and Van Laethan et al.[7] used a pyrometer to measure the temperature of hot glass. Attempts have also been made to determine steady temperature distributions in glass using interferometric data.[8] Temperatures obtained from interferometric data yield the average steady temperature along the optical path, but one cannot determine a truly local temperature interferometrically. The attempts to determine the internal glass temperatures using noncontact techniques have been motivated both by the fact that optical methods seem to be the only practical approach for temperature measurement in a production environment, and by the problems encountered in obtaining low-thermal contact resistance with contact instrumentation. However, until suitable optical methods are further developed, the only solution presently available to obtaining reliable internal temperature data is through the careful application of contact instrumentation.

Temperature measurements in glass using thermocouples or resistance thermometers are very difficult to obtain, especially for dynamic conditions where the response of the thermocouple is almost completely determined by thermal contact resistance. Serious complications also arise when using a bonding agent to secure the thermocouple to the glass. The bonding agents are usually some type of ceramic cement. A ceramic cement adds material around the thermocouple junction, having radiation and thermal properties significantly different from the glass. This can cause errors in the measured temperatures, due to perturbation of the radiation field in addition to the conduction and storage of heat by the thermocouple wire. It is easy to see that great difficulties are encountered when attempting to obtain temperature measurements in glass, and that these problems are particularly acute for dynamic conditions.

To minimize the effects mentioned above, a thermocouple installation method was developed which allows the placement of thermocouples on the surface and throughout the interior of glass test plates that assures excellent thermal contact, does not require the use of a bonding agent, and minimizes the disturbance of the radiation field by the thermocouple wires. This method (discussed below) requires fusion of the thermocouples to the glass. Fusing the thermocouples to the glass is difficult to accomplish, but yields exceptional measurement reliability.

Experimental Apparatus and Test Procedure

The test procedure consisted of heating a test plate to an initial temperature near the softening point (approximately 550°C) and then quickly transferring it to a lower temperature environment. The plate temperature distribution was then monitored while it cooled by natural convection and radiant heat exchange with the laboratory ambient from the front surface, and by natural convection and radiant exchange with a large heater positioned ~38 mm from the rear test plate surface. A schematic of model of this system is shown in Fig. 1. The data was recorded using a Hewlett Packard 3852A Data Acquisition/Control Unit. The thermocouple voltages were measured using a Hewlett Packard 44701A integrating voltmeter, and temperature data were obtained approximately every 10 s. Data acquisition was terminated automatically during each run when the test plate temperature reached a lower cutoff limit. The lower cutoff limit was generally selected to be ~300°C. The temperatures of the laboratory ambient and surroundings T_{a1}, T_{s1}, were for all practical purposes constant at 22°C for the duration of all tests. The heater surface temperature T_{s2} and ambient temperature T_{a2} were maintained at 240°C throughout the tests. The heater consisted of a 1250-W element, insulated using glass fiber insulation at the rear surface. The heater surface temperature was uniform within ±0.5°C. The surface of the heater was coated with EPC 2200 (3M Corporation) which has an emissivity of 0.93.

An electric furnace equipped with a convection fan to provide well-stirred cavity conditions was used to heat the test plates. The test plate shuttle mechanism, shown schematically in Fig. 2, held the test plate in a vertical position during both the heating and cooling process. The test plate was easily transported from the furnace interior to the test position (a distance of approximately 0.41 m) in less than 1 s.

Three thermocouples were used on each test plate. The thermocouples were installed in the front surface, rear surface, and at the center plane of each plate. The plates were approximately 200-mm square, and the thermocouple junctions were positioned approximately 12 mm from the center of the plate on the perpendicular bisector of the plate edge

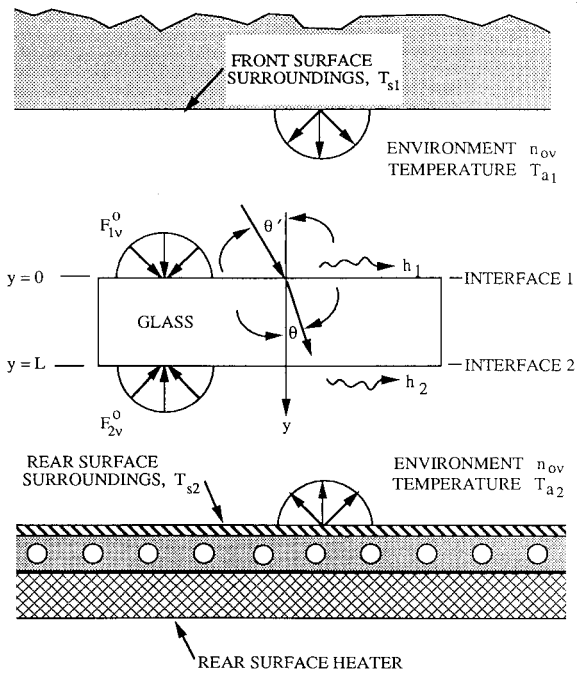

Fig. 1 System model schematic.

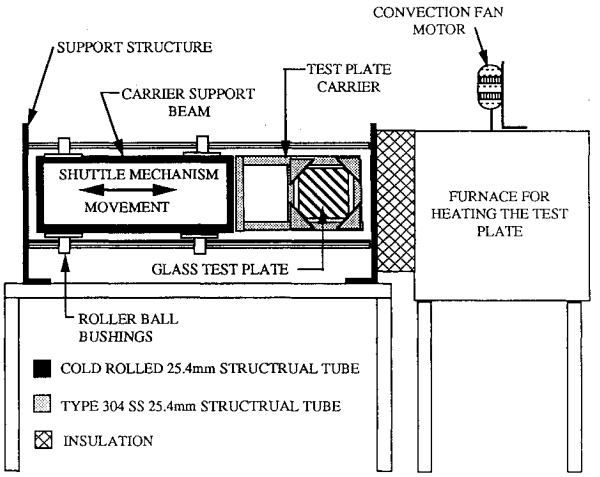

Fig. 2 Schematic of test plate shuttle mechanism and furnace.

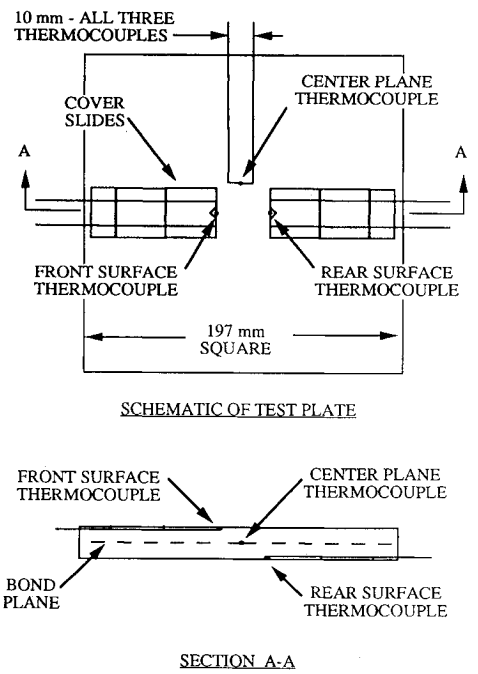

Fig. 3 Test plate schematic.

with a 90-deg clockwise rotation between each successive lateral station. A typical test plate and thermocouple placement is shown in Fig. 3. The basic approach of test plate fabrication was to fuse two glass plates into a single piece. The fusion process results in the thermocouples being engulfed by and bonded to the glass. The first step in the preparation of a test plate for fusion was to etch semicircular channels (using hydrofluoric acid) approximately 0.25 mm in diameter at the locations selected for the thermocouples. The test plate was assembled by installing the center plane thermocouple and placing a tiny drop of cyanoacrylate (super glue) cement at two diagonally opposite corners of the plates to hold them securely together while the surface thermocouples were installed. At the temperatures required for fusion, the cyanoacrylate cement decomposes and evaporates. The surface thermocouples were held in place prior to their fusion onto the surface using 18-mm square by 0.5-mm-thick glass cover slides, which also were secured to the plate using a tiny drop of cyanoacrylate cement. To fuse the two glass plates into a single unit, they were heated in a helium atmosphere to a temperature of ~650°C. While the fusion process was in progress, the temperature was monitored using the thermocouples installed on the plates. Additional details of the shuttle mechanism and the test plate fabrication can be found in Ref. 9.

Prediction of Temperature Distribution in Flat Glass

The system considered in the formulation of the energy equation model for a glass plate exchanging energy with its environment is as shown in Fig. 1. The glass plate exchanges heat by convection and radiation with the surroundings and environment on both sides of the plate. The term "surroundings" is used here in reference to parameters associated with radiant heat exchange, and the term "environment" is used in reference to parameters associated with the convective heat transfer from the glass. For example, on each side of the plate the convective environment temperatures are shown as T_{a1}, T_{a2}, and the surroundings temperatures as T_{s1}, T_{s2}. Heating or cooling at each interface is then obtained by specifying the appropriate environment and surrounding boundary conditions.

The formulation of the energy equation for semitransparent materials such as glass must, of course, properly account for the radiative energy transfer across the interfaces as well as throughout the interior of the glass. Modeling the radiative energy transfer across the interfaces and throughout the interior using rigorous radiative transfer theory has been reviewed by Viskanta and Anderson.[3] The following assumptions were used to develop the model equations describing this system:

1) The glass is in local thermodynamic equilibrium, therefore, Planck's and Kirchhoff's laws are valid.

2) Heat transfer by conduction, convection, and radiation occurs only in the y direction normal to the plate interfaces.

3) The glass is isotropic, homogeneous, and able to absorb and emit, but not scatter, thermal radiation.

4) The thickness of the glass is much greater than the radiation wavelength, making coherence effects negligible.

5) The glass is semitransparent to radiation for wavelength $\leq \lambda_c$, and opaque for wavelength $\lambda \geq \lambda_c$.

6) The variation of the refractive index in the glass with temperature is negligible over the temperature range of 200–600°C compared to the variation with wavelength.

7) The variation of radiation and thermophysical properties with wavelength and temperature are known.

Employing assumption 2, the transient one-dimensional energy equation for stationary glass plate is

$$\gamma C \frac{\partial T}{\partial t} = \frac{\partial}{\partial y}\left(k \frac{\partial T}{\partial y}\right) - \frac{\partial F_y}{\partial y} \tag{1}$$

where F_y denotes the radiative flux in the y direction. The solution of the energy equation requires the specification of an initial temperature distribution $T(y,0) = T_0(y)$ and boundary conditions at each interface of the glass plate. The boundary conditions at each interface are obtained from energy balances at each interface.

The interface energy balances provide the following relations for the boundary conditions at $y = 0$ and $y = L$, respectively:

$$k \frac{\partial T}{\partial y}\bigg|_1 = \pi\varepsilon\{g[\nu_1, \nu_2, T(0)]I_b[T(0)] - g(\nu_1, \nu_2, T_{s1})I_b(T_{s1})\} + h_1[T(0) - T_{a1}] \tag{2}$$

$$-k \frac{\partial T}{\partial y}\bigg|_2 = \pi\varepsilon\{g[\nu_1, \nu_2, T(L)]I_b[T(L)] - g(\nu_1, \nu_2, T_{s2})I_b(T_{s2})\} + h_2[T(L) - T_{a2}] \tag{3}$$

where

$$g(\nu_1, \nu_2, T) = \left[\left(\int_0^{\nu 1} I_{b\nu}(T)\, d\nu - \int_0^{\nu 2} I_{b\nu}(T)\, d\nu\right) \Big/ \int_0^{\infty} I_{b\nu}(T)\, d\nu\right] \tag{4}$$

is the blackbody fraction. The frequencies ν_1 and ν_2 indicate the spectral region where the glass may be considered opaque. The use of frequency, rather than wavelength, is convenient here since the frequency of electromagnetic energy does not change as it traverses the boundary between substances (such as air and glass) having different refractive indices.[10] Recall also that the frequency and wavelength values may be readily interchanged using the familiar relation $\lambda\nu = c$. The hemispherical emittance ε is for the spectral region where the glass is considered opaque. The convective heat transfer coefficient is represented by h, as is readily apparent from the context of Eqs. (2) and (3). If the glass is "hot" relative to the surroundings, the term $I_b(T_s)$ may be neglected as being small relative to $I_b[T(0)]$ or $I_b[T(L)]$.

The solution of Eq. (1) requires the determination of the radiant energy flux in the y direction F_y. Expressions for the radiative energy flux F_y, given as functions of the optical depth $\tau_\nu(y) = \int_0^y \kappa_\nu \, dy$ and local temperature, are provided by Viskanta and Anderson.[3] These expressions, which are presented below, were developed using the assumptions that the index of refraction is independent of temperature, that Bouguer's law[11] describes the absorption by the medium, and that the Fresnel equations[10] and Snell's Law[10] describe the reflection and refraction at the glass-air interfaces. The use of the Fresnel equations and Snell's Law carry with them the condition of optically smooth interfaces. It should be noted that when the index of refraction of the medium n_ν is greater than that of the surroundings $n_{0\nu}$, which is the case for glass immersed in air, Snell's Law ($n_{0\nu} \sin\theta' = n_\nu \sin\theta$) requires condensation by refraction across the interface. The impinging external radiant flux is condensed into the region between $\theta = 0$ and the critical angle θ_c given by $\theta_c = \sin^{-1}(n_{0\nu}/n_\nu)$. By using $\cos^2(\theta_c) = \mu_c^2 = 1 - (n_{0\nu}/n_\nu)^2$, the angular integration to determine the internal radiation flux originating from an external source is only necessary over the interval $\mu_c \le \mu \le 1$.

The evaluation of the internal radiant flux in a semitransparent material provided by Viskanta and Anderson[3] includes for both collimated and diffuse radiant fluxes incident on the interfaces of the medium. The expressions presented here have been restricted to diffuse incident flux on both interfaces of the glass plate as shown in Fig. 1. Following Viskanta and Anderson,[3] the expression for $F_\nu(\tau_\nu)$ has been separated into two parts, $F_{C\nu}(\tau_\nu)$ and $F_{H\nu}(\tau_\nu)$, to provide clarity

$$F_{c\nu}(\tau_\nu) = 2[F^0_{1\nu}T_{3,1}(\tau_\nu) + F^0_{2\nu}T_{3,21}(\tau_{L\nu} + \tau_\nu)](n_\nu/n_{0\nu})^2 - 2[F^0_{1\nu}T_{3,12}(2\tau_{L\nu} - \tau_\nu) + F^0_{2\nu}T_{3,2}(\tau_{L\nu} - \tau_\nu)](n_\nu/n_{0\nu})^2 \quad (5)$$

with

$$T_{n,i}(\tau) = \int_{\mu_c}^1 [1 - \rho_i(\mu')]\exp(-\tau/\mu)\mu^{n-2}\, d\mu/\beta(\tau_L, \mu) \qquad i = 1, 2 \quad (6)$$

$$T_{n,ij}(\tau) = \int_{\mu_c}^1 [1 - \rho_i(\mu')]\rho_j(\mu)\exp(-\tau/\mu)\mu^{n-2}\, d\mu/\beta(\tau_L, \mu) \qquad i = 1, 2, \quad j = 1, 2, \quad i \neq j \quad (7)$$

$$\beta_\nu(\tau_{L\nu}, \mu) = 1 - \rho_{1\nu}(\mu)\rho_{2\nu}(\mu)\exp(-2\tau_{L\nu}/|\mu|) \quad (8)$$

In Eq. (5), the transmission across the interface from external sources are accounted for through the functions $T_{n,i}(\tau)$, $T_{n,ij}(\tau)$. The function $\beta_\nu(\tau_{L\nu}, \mu)$ accounts for multiple internal reflections

$$F_{H\nu}(\tau_\nu) = 2\pi \left\{ \int_0^{\tau_{L\nu}} n_\nu^2 I_{b\nu}[T(\eta)][R_{2,1}(\tau_\nu + \eta) + R_{2,12}(2\tau_{L\nu} + \tau_\nu - \eta) - R_{2,2}(2\tau_{L\nu} - \tau_\nu - \eta) - R_{2,21}(2\tau_{L\nu} - \tau_\nu + \eta) + \text{sign}(\tau_\nu - \eta)E_2(|\tau_\nu - \eta|)] \right\} d\eta \quad (9)$$

with

$$R_{n,i}(\tau) = \int_0^1 \rho_i(\mu)\exp(-\tau/\mu)\mu^{n-2}\, d\mu/\beta(\tau_L, \mu), \qquad i = 1,2 \quad (10)$$

$$R_{n,i}(\tau) = \int_0^1 \rho_i(\mu)\rho_j(\mu)\exp(-\tau/\mu)\mu^{n-2}\, d\mu/\beta(\tau_L, \mu) \qquad i = 1, 2, \quad j = 1, 2, \quad i \neq j \quad (11)$$

$$\text{sign}(\tau - \eta) = +1 \quad \text{if} \quad \tau > \eta$$

$$\text{sign}(\tau - \eta) = -1 \quad \text{if} \quad \tau > \eta$$

In Eq. (9), the flux contribution from internal emission is accounted for through the $I_{b\nu}[T(\eta)]$ function. Integration of $F_\nu(\tau_\nu)$ over the frequency range where the material exhibits semitransparent behavior yields the internal radiative flux at position y. Computation of the radiative flux throughout the interior of the plate provides the definition of F_y from which $\partial F_y/\partial y$ required in Eq. (1) may be evaluated.

Physical Properties of Glass Plate

To predict the temperature distribution in the glass plate, using the rigorous formulation of the energy equation, requires the utilization of numerical methods along with specification of γ, C, k, and the spectral absorption coefficient κ_ν. The density of the soda-lime glass used in the prediction computations was experimentally determined. The measured densities were all very consistent at a value of 2514.8 ± 0.1 kg/m^3. The specific heat for soda-lime glass used in the solution of the energy equation was determined using the method of Sharp and Ginther[12] for the typical soda-lime glass composition.[13] Thermal conductivity, however, is much more difficult to determine for glass and has been studied by many researchers.[14] For many years the thermal conductivity quoted for semitransparent materials such as glass was the "apparent" thermal conductivity. Virtually all of the thermal conductivity data taken prior to the late 1950s is apparent thermal conductivity, and must be used with caution unless the conditions under which the tests were made are well known and understood. An empirical equation proposed by Endrys and Turzik,[15] $k(T) = 0.722 + 0.00158T$, where k is in W/m°C, and T is in °C, was used to model the true thermal conductivity of the glass test plates. The true thermal conductivity is not as sensitive to glass composition as is the combination of thermal and radiation (apparent) conductivity, since the phonon contribution is relatively small. At high temperatures the radiant energy transfer is large compared to the molecular contribution, and absorption/emission dominates the overall energy transfer.

The variation of the spectral absorption coefficient with wavelength is not a smooth continuous function and must be approximated using a model capable of accounting for the rapid "jumps" seen in absorption data. The most straightforward procedure to model the rapid changes of the absorption coefficient is to use a band model approximation. In the

band model approach a series of finite spectral intervals are used where the absorption coefficient is assumed constant at the average value in each region. The average value of the absorption coefficient in each band is then used in Eqs. (5) and (9) to compute the flux for each spectral interval of the band model. The total flux at each grid point is the sum of the values found for each band.

Sensitivity studies were performed over a large range of spectral bands (up to 32 bands were investigated) to determine the number necessary to adequately model the absorption data.[9] The investigation indicated that five bands was sufficient to model the absorption coefficient over the spectral range of 0–5μm. All results reported here were obtained utilizing the five-band spectral model for the absorption coefficient of soda-lime glass determined from the data reported by Rubin,[16] which is shown in Fig. 4. Using more than five bands produced no significant change in the predicted results and required increased computation time.

Method of Solution

The complexities of the energy equation, when radiative transfer has been included, require the use of numerical methods for solution. The numerical method employed consisted of first transforming the energy equation and boundary conditions to a dimensionless form, then discretizing using finite-difference approximations. An implicit time-marching technique was used for the solution of the finite-difference equations. The nature of F_y term requires an "internal iteration" to be performed at each time interval to produce consistency between the temperature profile and the radiation field. This iteration could be viewed as adding an explicit character, and the approach could be viewed as both "implicit/explicit," but the solution method is predominantly implicit.

Evaluation of the reflection ($R_{n,j}$, $R_{n,ij}$) and the transmission ($T_{n,j}$ $T_{n,ij}$) functions were accomplished using a single application of 16-point-G quadrature applied over the integration interval. The exponential nature of these functions requires careful numerical integration to produce satisfactory results. A check was made by using multiple applications of the 16-point quadrature in smaller subintervals, and summing the results to determine if the single 16-point quadrature application for evaluation of these functions was satisfactory. No significant benefit in evaluating these functions was observed when using multiple intervals relative to the single 16-point application.

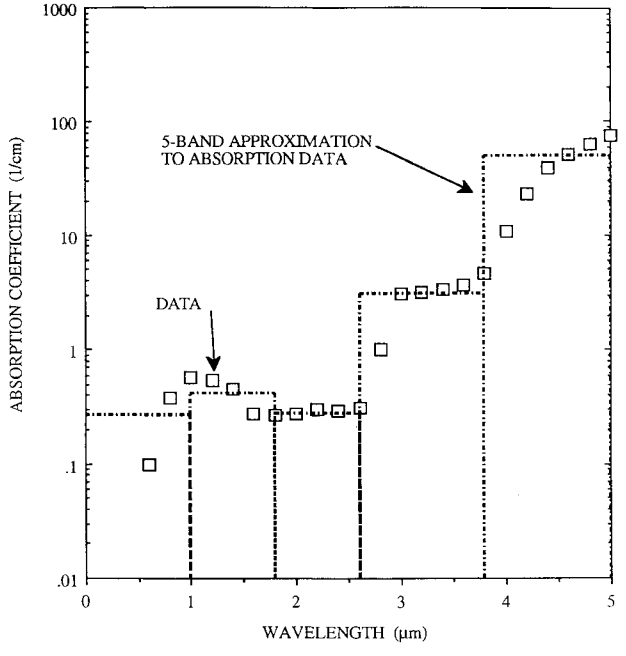

Fig. 4 Spectral band model and absorption coefficient for soda-lime glass.

The solution sensitivity to the selection of time step, node spacing, and spectral band width was extensively studied to determine the necessary conditions to achieve time step, grid spacing, and spectral band width independence. The node spacing used for the predictions were 0.371, 0.338, and 0.292 mm, respectively for the 3.71-, 6.76-, and 11.68-mm test plates. This node spacing produces approximately the same optical thickness between grid points in each plate while maintaining a convenient number of nodes.

Evaluation of the internal radiant flux requires specification of the temperature at each grid point. To maintain consistency between the temperature profile and the radiant flux, an iteration at each time is necessary. The implicit time-marching technique, with the internal iteration to maintain consistency between the temperature profile and radiant flux, provides a solution method which is practically insensitive to the time step. The time steps used were generally selected to correspond closely with the measured data. Computations at intermediate times to provide solution stability or time-step independence was not necessary. A typical run on a SUN SPARC station 1+ takes approximately 2 min for 40 time steps using a 6.76-mm plate thickness. Additional details concerning the solution method can be found in Ref. 9.

Comparison of Predicted and Measured Temperatures

The internal radiative energy transfer in glass is a bulk phenomenon, as discussed above, and verification of the energy equation model predictions required testing a range of plate thickness. Plates 3.71-, 6.76-, and 11.68-mm thick were selected for the testing. These plate thicknesses are representative of those typically used in high-temperature window applications.

Prediction of the test plate temperatures by solving the energy equation for glass requires the specification of the convective heat transfer coefficient at the test plate surfaces to appropriately define the convective boundary condition. Correlations for natural convection heat transfer from a vertical plate were not appropriate in this case because the shuttle mechanism's test plate carrier formed a frame around the test plate which was 25.4-mm wide. The presence of the frame produced flow patterns on the plate surface which were different from those for a vertical plate immersed in an infinite volume of fluid.[16] The influence of the test plate carrier frame made it necessary to determine the convective heat transfer coefficient experimentally.

The convective heat transfer coefficient at the plate surface, as installed in the shuttle mechanism, was determined using a thin (1.85 mm) glass test plate. When the plate is thin enough, internal conduction/radiation can be neglected, and the energy transfer from the plate is due to convection from the surface and by radiation at wavelengths longer than 5.0 μm where the glass can be considered opaque. When convective heat transfer and radiation from an opaque surface dominate the cooling, the convection coefficient can be determined by measuring the cooling rate of the test plate and employing a lumped system analysis. The cooling rate of a 1.85-mm plate was determined experimentally, and the convective heat transfer coefficient was found to be nearly constant at 4.25 W/m^2°C over the temperature range of 250–550°C. This value is approximately one-half that expected from published correlations for a vertical plate without the 25.4-mm test plate carrier frame surrounding it.[17] The convective heat transfer coefficient of 4.25 W/m^2°C determined for the plate was used in all predictions for the test plate temperature distributions.

Radiative energy transfer is the dominate factor in the cooling of high-temperature windows. Appreciation for the importance of the radiant energy transfer can be immediately gained by inspecting Fig. 5. In the figure, the temperatures

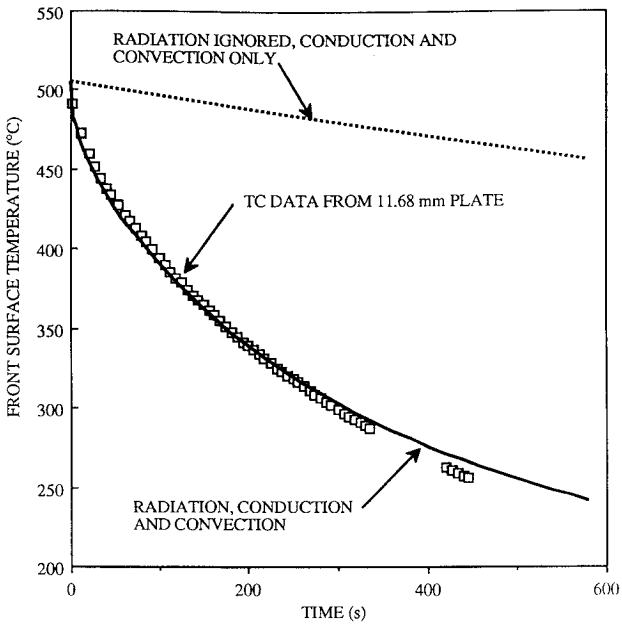

Fig. 5 Comparison of predicted vs measured 11.68-mm plate front surface temperatures with and without radiation effects.

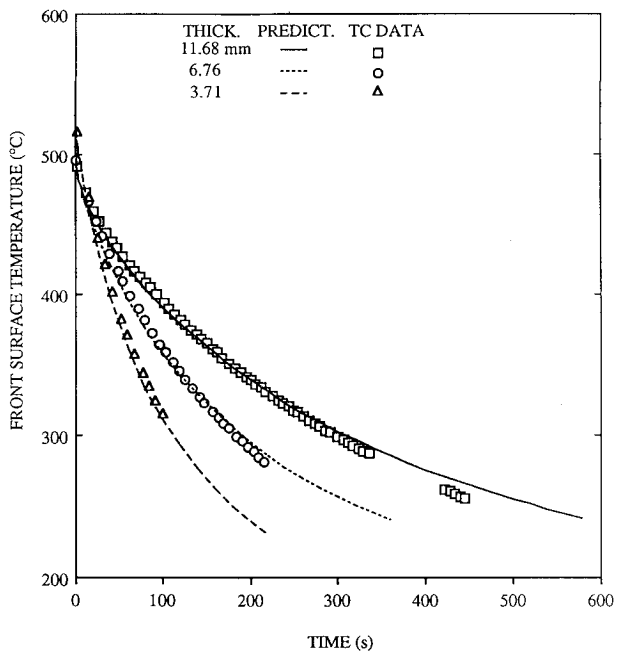

Fig. 6 Comparison of front surface predicted and measured temperatures.

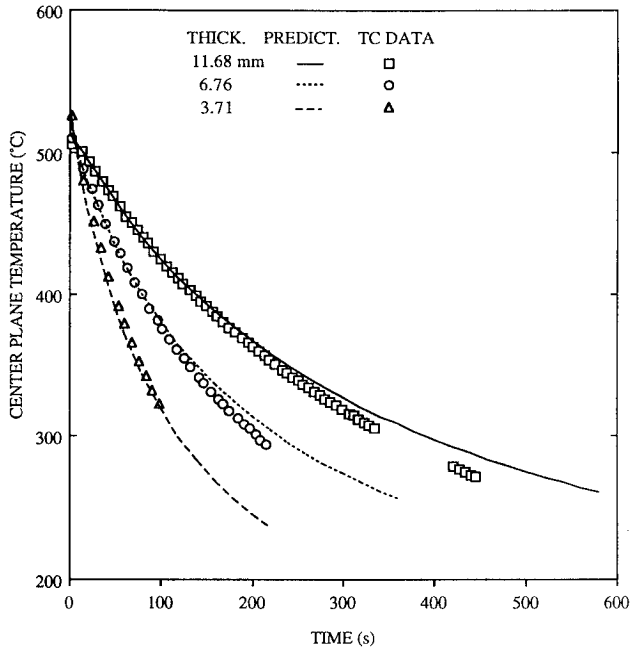

Fig. 7 Comparison of predicted and measured plate center plane temperatures.

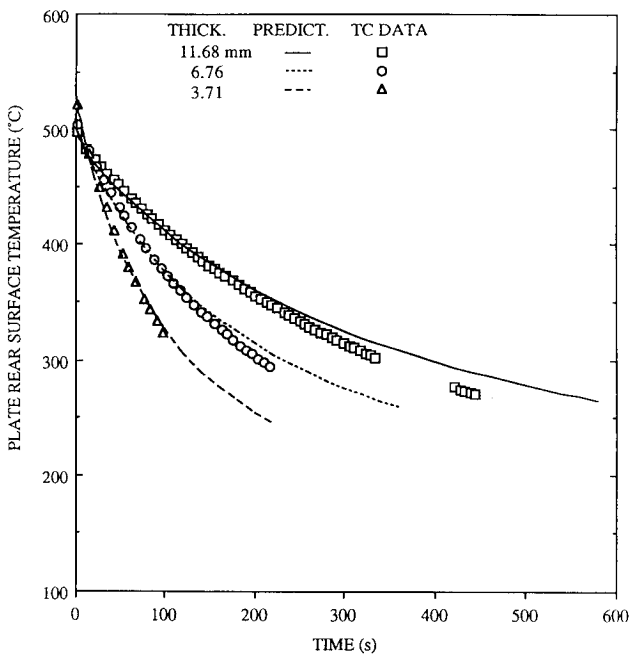

Fig. 8 Comparison of predicted and measured plate rear surface temperatures.

obtained from the front surface thermocouple on the 11.68-mm test plate are compared with predicted surface temperatures when radiation has been both included and ignored. When the radiative energy transfer is ignored in the energy balance, as shown by the "radiation ignored, conduction and convection only" curve, very poor correlation with the data is obtained. Properly accounting for the radiative energy transfer produces very good agreement between prediction and measurement as demonstrated by the "radiation, conduction and convection" curve in Fig. 5.

The comparison of predicted temperatures with the thermocouple data from each test plate for the front surface, center plane, and rear surface are shown in Figs. 6–8. The deviations between the thermocouple measurements and predictions are generally less than 10°C. The center-to-front surface temperature difference deviation of the predictions relative to the measurements are displayed in Fig. 9. This is a very critical comparison, as the magnitude of the center-to-surface temperature differences are quite small. The surface-to-center temperature difference is the largest for the 11.68-mm plate. At selected times during the cooling process, the internal plate temperatures vs thickness, predicted for the 11.68-mm plate, are given in Fig. 10 to provide an illustration of how the internal temperature profile changes with time. Both Figs. 9 and 10 show that the differences between the surface and the center plane temperatures remain relatively small throughout the cooling process. A trend, however, can be seen in Fig. 9 between the data and the predictions. The predicted center-to-front surface temperature difference is always slightly greater than that indicated by the thermocouple data, and the deviations increase progressively with plate thickness. The smaller center-to-surface temperature difference from the thermocouple data indicates that the actual

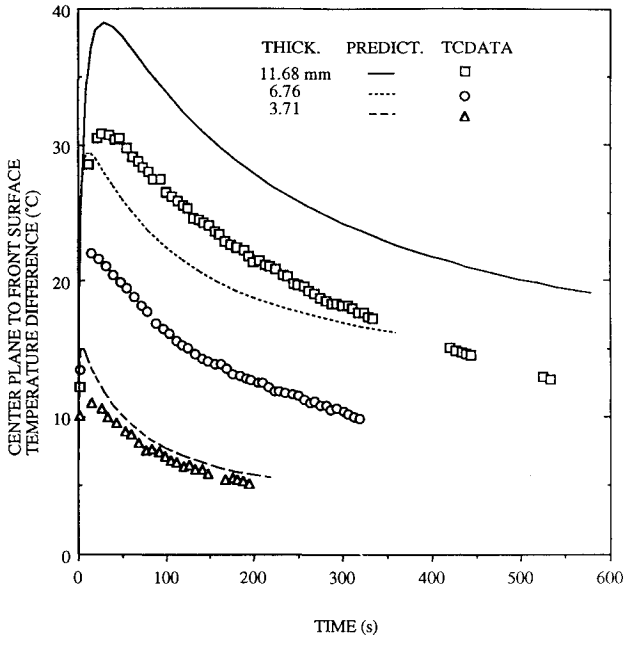

Fig. 9 Comparison of the predicted and measured center plane-to-front surface temperature difference.

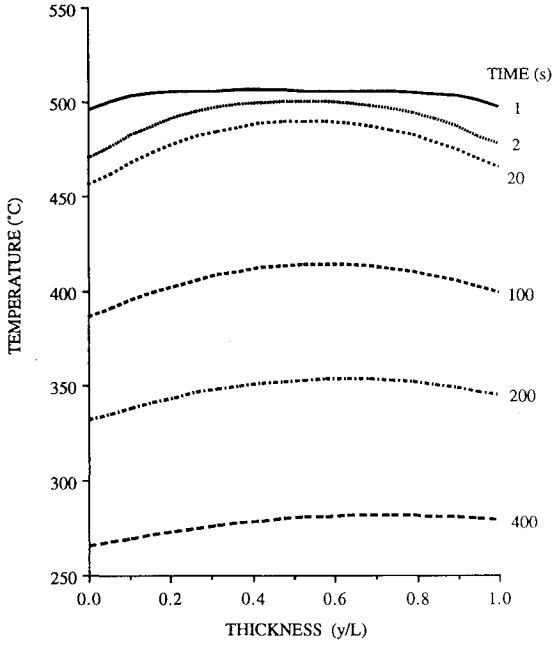

Fig. 10 Predicted internal temperatures profiles for the 11.68-mm plate cooling from 500°C with heating from an external source at $y/L = 1$.

temperature profile of the 11.68-mm plate is even flatter than that shown in Fig. 10. Even though the temperature profiles are relatively flat, the effect of the rear surface heater can be observed, since the rear surface temperature is always greater than the front surface temperature.

The deviations between the predictions and the data can be mostly attributed to differences between the thermophysical properties of the test plate and the correlations used in the solution of the energy equation. Sensitivity studies were conducted to determine the most probable cause of this deviation. These studies indicated that the thermal conductivity of the glass used in the solution of the energy equation was slightly too low. Equivalent energy transfer to the surface by conduction required higher temperature differences in the model predictions than indicated by the thermocouple measurements. The rate of change with time of predicted surface-to-center temperature difference and that obtained from the thermocouple data are very similar in the early portion of the cooling process. The 11.68- and 6.76-mm plate data for the later part of the cooling process shows an increasing deviation between the predicted and measured data. In the early portion of the cooling process, radiation dominates the energy transfer. As the plate temperature drops, conduction becomes the dominant mechanism of energy transfer from the plate, and the deviation between the thermal conductivity model used in the prediction and the actual thermal conductivity of the plate becomes increasingly more important. The increasing deviation is due to the thermal conductivity being too low, and results in a larger predicted temperature difference required to transfer energy to the plate surface from its interior. The prediction for the 3.71-mm plate shows much better agreement with the data since the plate is thin enough that the center-to-surface temperature differences always remains small, minimizing the effect of the deviation between the actual plate thermal conductivity and that used in the model calculations. The rate of change of plate temperature with time is nearly identical for both the test data and the prediction. Since the rate of change is nearly the same in both instances, it can then be inferred that the specific heat of the glass was modeled reasonably well, and that the rate of energy transfer from the plates was nearly the same for both prediction and experiment.

The thermal conductivity is the thermophysical property having the highest level of uncertainty. The agreement between the predicted and measured temperatures can be considerably improved, relative to the thermocouple data shown in Fig. 9, by increasing the thermal conductivity. In the sensitivity studies conducted to determine the most probable cause of the deviation, the thermal conductivity from the Endrys and Turzik[15] relation was arbitrarily increased by 20%. The 20% increase of thermal conductivity brought the measured and predicted center-to-surface temperature differences, on average, to within 3°C or less,[9] but still did not provide the desired rate of change with plate temperature necessary to match the data throughout the cooling process. To obtain better agreement between the data and prediction for glass thicker than 3.71 mm, a thermal conductivity model having both an increased magnitude and an adjustment in the rate of change with temperature relative to the Endrys and Turzik[15] relation is required. Further discussion of the center-to-surface temperature difference relative to the true thermal conductivity characteristics of the glass can be found in Mann et al.[18]

Conclusions

The dynamic internal temperature distributions in glass undergoing heating and cooling processes may be predicted to within ~10°C, using the combined conduction-radiation heat transfer model. The agreement between the model predictions and the test data for all plates between 3.7–11.68-mm thick indicate that the energy equation model formulated using radiative transfer theory is capable of accurate temperature distribution prediction for a wide range of glass thickness. The deviations seen between the model predictions and the measured temperatures are attributed primarily to the result of the uncertainty in the thermal conductivity. Using the energy equation model described here, uncertainties in temperature predictions for semitransparent materials (assuming care has been taken to obtain time step, grid, and spectral band model independent solutions) will primarily result from uncertainties in the knowledge of the convective heat transfer boundary conditions and the glass thermophysical properties, rather than unsatisfactory accounting of radiant energy transfer.

References

[1]Holman, R. A., "Mold Temperature Measurement for Glass-Pressing Processes," *Applications of Radiation Thermometry, ASTM*

STP 895, edited by J. C. Richmond and D. P. DeWitt, American Society for Testing and Materials, Philadelphia, 1985, pp. 67–73.

[2]Barber, R., "Glass Industry Applications," *Theory and Practice of Radiation Thermometry*, edited by D. P. DeWitt and G. D. Nutter, Wiley, New York, 1988, pp. 973–1043.

[3]Viskanta, R., and Anderson, E. E., "Heat Transfer in Semitransparent Solids," *Advances in Heat Transfer*, Vol. 11, edited by J. P. Hartnett and T. F. Irvine, Jr., Academic Press, New York, 1975, pp. 318–441.

[4]Ping, T. H., and Lallemand, M., "Transient Radiative-Conductive Heat Transfer in Flat Glasses Submitted to Temperature, Flux and Mixed Boundary Conditions," *International Journal of Heat and Mass Transfer*, Vol. 32, No. 5, 1989, pp. 795–810.

[5]Gardon R., "Calculation of Temperature Distribution in Glass Plates Undergoing Heat-Treatment," *Journal of the American Ceramics Society*, Vol. 44, No. 6, 1958, pp. 200–209.

[6]Beattie, J. R., and Coen, E., "Spectral Emission of Radiation by Glass," *British Journal of Applied Physics*, Vol. 11, No. 4, 1960, pp. 151–157.

[7]Van Laethan, R., Leger, L. G., Boffé, M., and Plumet, E., "Temperature Measurement of Glass by Radiation Analysis," *Journal of the American Ceramics Society*, Vol. 44, No. 8, 1961, pp. 321–332.

[8]Viskanta, R., "Infrared Radiation Techniques for Glass Surface and Temperature Distribution Measurements," *IEEE Transactions Ind. Appl.*, IA-1, Vol. 5, No. 5, 1975, pp. 494–505.

[9]Field, R. E., "Spectral Remote Sensing of the Temperature Distribution in Glass," Ph.D. Dissertation, Purdue Univ., West Lafayette, IN, 1989.

[10]Hect, E., and Zajac, A., *Optics*, Addison-Wesley, Reading, MA, 1974.

[11]Siegel, R., and Howell, J. R., *Thermal Radiation Heat Transfer, Second Edition*, Hemisphere, New York, 1981.

[12]Sharp, D. E., and Ginther, L. B., "Effect of Composition and Temperature on the Specific Heat of Glass," *Journal of the American Ceramics Society*, Vol. 34, No. 9, 1954, pp. 260–271.

[13]Blazek, A., Endrys, J., Kada, J., and Stanek, J., "Thermal Radiation Conductivity of Glass-Influence of Glass Composition on Its Heat Transmission," *Glastechnische Breichte*, Vol. 49, No. 4, 1976, pp. 75–81.

[14]Touloukian, Y. S., Powell, R. W., Ho, C. Y., and Klemens, P. G., *Thermophysical Properties of Matter*, Vol. 2, Plenum Press, New York, 1970.

[15]Endrys, J., and Turzik, D., "Die Temperaturverteilung in Glas bei Stationerem Zustand," *9. Internationale Baustoff-und Silikattagung Weimar*, Sektion 5, Hochschule für Architektur und Bauwesen, Weimar, 1985, pp. 35–40.

[16]Rubin, M., "Optical Properties of Soda-Lime Silica Glasses," *Solar Energy Materials*, Vol. 12, No. 4, 1985, pp. 275–288.

[17]Chapman, A. J., *Heat Transfer*, Macmillan, New York, 1967, pp. 356–368.

[18]Mann, D., Field, R. E., and Viskanta, R., "Determination of Specific Heat and True Thermal Conductivity of Glass from Dynamic Temperature Data," *Wärme- und Stoffübertragung*, Vol. 27, No. 4, 1992, pp. 225–231.